Published in final edited form as:
Biochemistry. 2011 December 27; 50(51): 11001–11008. doi:10.1021/bi2014486.

Structure, dynamics and binding of the LA45 module pair of the Low Density Lipoprotein Receptor suggest an important role for LA4 in ligand release

Miklos Guttman and **Elizabeth A. Komives***
Department of Chemistry and Biochemistry, University of California San Diego, 9500 Gilman Dr. La Jolla, CA 92093-0378

Abstract

The Low Density Lipoprotein Receptor (LDLR), the primary receptor for cholesterol uptake, binds ligands through its seven LDL-A modules (LAs). We present NMR and ligand binding measurements on the fourth and fifth modules of the LDLR (LA45), the modules critical for ApoE binding, at physiological pH. Unlike LA5 and all other modules in LDLR, LA4 has a very weak calcium affinity, which probably plays a critical role in endosomal ligand release. The NMR solution structure of each module in the LA45 pair only showed minor differences compared to the analogous domains in previously solved crystal structures. The 12 residue linker connecting the modules, though slightly structured through an interaction with LA4, is highly flexible. Although no inter-module NOEs were detected, chemical shift perturbations and backbone dynamics suggest crosstalk between the two modules. The ligand affinity of both modules is enhanced when the two are linked. LA4 is more flexible than LA5 and remains so even in the module pair, which likely relates to its weaker calcium-binding affinity.

The low density lipoprotein receptor family is critical for the uptake of cholesterol containing lipoprotein particles. The best characterized of these is the low density lipoprotein receptor (LDLR), which contains seven LDL-A (LA) modules that mediate ligand interactions (Fig. 1).[1] Once ligand binding occurs, the receptor-ligand complex is endocytosed and ligand is released. Upon endocytosis the lower pH within the endosome triggers an intra-molecular interaction between the LA modules and the β-propeller domain causing ligand release by way of displacement.[2] However the significantly lower pH and calcium ion concentration within the endosome has also been suggested to promote ligand release independent of this displacement mechanism.[3]

The structures of several LA modules from LDLR and related receptors have been solved both by X-ray crystallography [2,4,5,6] and NMR [7,8,9]. All of these share a conserved disulfide pattern and a calcium binding site [10,11] resulting in a common fold. Specificity of ligand binding is thought to be determined mainly through exposed nonconserved residues.[1] Each module is linked to its neighbor by a 4 or 5 residue linker, except for the fourth (LA4) and fifth (LA5) LDLR modules, which have a 12 residue linker. It is believed that LA modules behave independently of their neighbors like beads on a string.[12,13,14,15]

*Corresponding author: ekomives@ucsd.edu or 858-534-3058.

Data Deposition: Atomic coordinates of the 20 lowest energy structures of LA45 have been deposited in the Protein Data Bank, www.rcsb.org (PDB ID code: 2lgp).

Supporting information
Supporting Information is available as indicated in the text. This material is available free of charge via the Internet at http://pubs.acs.org.

The LA modules in LDLR have high affinity for several physiological ligands including Apolipoprotein E (ApoE)-containing β-VLDL particles.[16] Ligand binding assays with recombinant LDLR from which single modules were deleted showed that LA5, and to a lesser extent LA4, were the key modules for mediating β-VLDL binding.[17] The same study showed that deletion of the extra long linker between LA4 and LA5 can affect the binding of certain ligands. The LA45 module pair was later shown to be the minimal unit of LDLR to bind β-VLDL-mimicking apoE•dimyristoyl-phosphatidylcholine (DMPC) particles *in vitro*.[18] The order of these critical modules is also important as swapping the position of LA5 in LDLR also impaired ligand binding.[19]

The structures of LA5 at low pH, LA34 complexed with domain 3 of the receptor associated protein (RAP), and the entire LDLR at endosomal pH have been solved,[2,4,6] but the structure and behavior of LA45 at physiological pH, presumably the form that binds ApoE, remain elusive.[20] Here we report the NMR structure, calcium binding properties, and backbone dynamics of the LA45 module pair revealing some unique properties of this critical module pair.

Methods

Protein Expression

LDLR LA fragments were cloned, expressed, purified and refolded as described previously.[21] Constructs containing LA4 were further purified by reverse phase HPLC (DELTA-PAK 300X19mm I.D. 15μm 300A C18, Waters) in 10mM NH_4OAc pH 5.5 containing 5mM $CaCl_2$ with a linear acetonitrile gradient (10–50%) at 10mL/min. For calcium binding studies LA constructs were re-purified with a 10% – 50% acetonitrile gradient using 0.1% trifluoroacetic acid (TFA) to remove calcium ions. Proteins were lyophilized and stored at −20°C. Masses of the final proteins were confirmed by MALDI-TOF (Voyager DESTR, Applied Biosystems) mass spectrometry. Size exclusion chromatography indicated that the refolded proteins were monomeric.

All of the LDLR ligands were prepared as ubiquitin fusions because this aided in solubility of the ApoE(130-149). A Ubiquitin (Ub) fusion vector was generated by cloning the DNA sequence for Ubiquitin into the Nco1 and BamH1 sites of vector pHis8.[22] RAPD3 (residues 252–357) was introduced between the BamH1 and Not1 sites to generate a His8-Ub-RAPD3 construct. The same strategy was used to generate His8-Ub-ApoE(130-149). A stop codon was inserted at the C-terminal end of Ub to generate a His8-Ub construct that was used to prepare free Ub as a negative control ligand. Proteins were produced in BL21-DE3 cells, grown in LB to OD_{600} 0.5, and induced with 0.1mM IPTG isopropyl-beta-D-thiogalactopyranoside (IPTG) for 4 hrs at 37°C. Cells were harvested, resuspended in TBS (50mM Tris pH 8.0 500mM NaCl), lysed by sonication, and the protein was purified by Ni-NTA (Qiagen), and size exclusion (Sephadex 75, GE healthcare) in 20mM Hepes pH 7.45, 150mM NaCl, 10mM $CaCl_2$, and 0.02% azide. For Ub-ApoE(130-149) and additional cation exchange step (monoS, GE healthcare) using a gradient of 0 to 750mM NaCl was necessary prior to size exclusion.

Isothermal titration calorimetry (ITC)

Calcium binding titrations were performed on a MicroCal VP-ITC calorimeter at 35°C. Dried protein was resuspended (250μM) in Chelex (BioRad)-treated buffer (20mM Hepes (pH 7.4), 150mM NaCl, 0.02% azide). Each protein was titrated with 2.5 mM $CaCl_2$ in the same buffer. LA4 titration was repeated using 5mM $CaCl_2$, at pH 7.4 and also at pH 5.2. Data were fit in Origin 6.0 (OriginLab).

NMR

NMR experiments were collected at 33°C on a 600 MHz Bruker AvanceIII spectrometer equipped with a cryoprobe. Dried proteins were dissolved to a final concentration of 0.7 – 1mM in 20mM D-18 HEPES (Cambridge Isotope Labs) (pH 7.45), 150mM NaCl, 5mM $CaCl_2$, 10% D_2O with 0.02% sodium azide. Backbone resonances were assigned with CBCA(CO)NH,[23] CBCANH,[24] and HNCO.[25] Side chain assignments were made with (H)CC(CO)NH,[26] 3D ^{15}N-separated NOESY-HSQC (200msec mixing time),[27] 3D ^{13}C-^{15}N separated HMQC-NOESY-HSQC (e.g. (H)CNH NOESY, 200msec mixing time), 3D HCCH TOCSY,[28] 3D HCCH COSY [29] and 3D ^{13}C-separated NOESY-HSQC (200msec mixing time) [30] spectra. The protein was dried and resuspended 100% D_2O (Cambridge Isotope Labs) twice, prior to collection of HCCH COSY, HCCH TOCSY and HCCH NOESY experiments. Spin systems for residues not visible in amide resolved experiments were assigned with the 3D HCCH-TOCSY and 3D HCCH-COSY and connectivity established with NOESY spectra. Spectra were processed in either NMRpipe [31] or Azara 2.7 (Wayne Boucher and the Department of Biochemistry, University of Cambridge) using maximum entropy reconstruction for the indirect dimensions in 3D experiments, and analyzed in Sparky.[32] RDCs for NH vectors were measured with HSQC-IPAP experiments [33] comparing an unaligned sample of 0.2mM LA45 against an identical sample containing 10mg/mL pf1 phage (Asla Biotech).

Structural Refinement

Peak lists from ^{13}C-NOESY, ^{15}N-NOESY and HCN-NOESY (200msec mixing time) were analyzed with Aria2 for iterative NOE assignments.[34] 50 dihedral angle restraints were obtained from analysis of NH, H, Hα, CO, Cα, and Cβ chemical shifts using TALOS.[35] 36 restraints to mimic the calcium coordination were added as described previously.[9] Hydrogen bond donors (6) were added based on protection in H/D exchange experiments, and acceptors identified from initial structures. The six disulfide restraints were initially set as distance restraints and later set as covalent bonds. Manually assigned NOEs (112) involving the linker region were used as additional restraints. Rhombic and axial components of the alignment tensor (0.49, 6.7 respectively) were estimated with the maximum likelihood approach [36] and RDC values were included as susceptibility anisotropy (SANI) restraints with an error estimate of 0.4Hz. 20 structures from initial refinement with no NOE (>0.5Å) or dihedral (>5°) violations were further refined using the distance geometry simulated annealing protocol in CNS 1.2,[37] with bona fide calcium restraints.[38] RMSDs were calculated with Superpose 1.0.[39] NMR assignments and relevant data have been uploaded to BMRB (accession number 16480), and coordinates have been deposited at the protein data bank (pdb accession 2lgp). The figures were made using Pymol.[40]

Backbone Dynamics

^{15}N uniformly labeled samples in the same NMR buffer were used to collect ^{15}N–{^{1}H}NOEs, ^{15}N T_1 and T_2 relaxation measurements at 33°C. Relaxation measurement delays ranged from 5 msec to 3 seconds (T1) and 14 to 182 msec (T2). Spectra with and without presaturation to determine the ^{15}N–{^{1}H}NOEs were collected in an interleaved manner with a 6 sec recycle delay. T_1 and T_2 relaxation measurements were fit to exponentials and errors were obtained from the uncertainty of the fit and from occasional duplicate points yielding similar uncertainties. The ^{15}N–{^{1}H}NOEs were calculated from the ratio of peak heights in duplicate and errors are the standard deviations. For H/D exchange experiments, 0.4mM ^{15}N labeled samples in the same NMR buffer were dried and resuspended in either 10% D_2O or 100% D_2O and a series of ^{1}H-^{15}N HSQCs were collected from 15 min to 2 hrs at 25°C. Data was processed with NMRpipe [31], and analyzed in Sparky.[32] Tensor 2.0 was used for model free fitting of relaxation data with 100 cycles of Monte Carlo simulations for error analysis [41]. Theoretical correlation times based on atomic

coordinates were calculated with HYDRONMR. [42] An atomic element radius (5.2 Å) was found to predict the observed value for LA5 (3.66nsec predicted vs. 3.68 measured) and was used for subsequent calculations on all constructs.

Ligand titrations

40nmol of dried ^{15}N labeled LA module(s) were resuspended in 400 μL of either 0.5mM Ubiquitin or Ub-RAPD3. The samples were mixed in ratios to yield several concentrations of RAPD3 between 0 and 500μM, and each was monitored by ^{1}H ^{15}N HSQC. Ub-ApoE(130-149) titrations were conducted in the same manner but with higher concentrations of titrant (>1mM). The chemical shifts were analyzed as a function of titrant in both dimensions, and ^{15}N shifts were scaled down by the $^{1}H/^{15}N$ gyromagnetic ratio (9.8). K_Ds and errors were calculated as described previously.[21,43]

Results

Refolding of LA4

The LDLR LAs each contain six cysteines that form three disulfide bonds, and it was therefore necessary to produce them in *E. coli* in an unfolded state and refold them under disulfide exchange conditions.[4] Unlike LA5 and LA3, LA4 did not efficiently refold to one disulfide-bonded isomer, in agreement with previous observations.[13] LA4 was isolated as a single peak by analytical HPLC with the expected mass, but the ^{1}H-^{15}N HSQC spectrum showed more than the expected number of cross peaks (56/41) indicating heterogeneity. Reverse phase HPLC purification in ammonium acetate at pH 5.5 with 5mM $CaCl_2$ resolved three species of LA4 (Fig. 2A). Since the mass of each species was that expected for LA4 (5118.7+/− 3Da measured vs. 5120.9 theoretical) it was likely that distinct disulfide bond isomers were present. Only the earliest eluting, major peak had a dispersed HSQC spectrum with even line shapes, reflective of a well-folded protein (Fig. 2B). Refolding of the tandem constructs of LA45 and LA345 resulted in similar amounts of misfolded species suggesting that contact with neighboring modules did not assist in the proper refolding of LA4.

Calcium binding

Calcium affinity of each module was measured by ITC. The binding isotherms of LA3 and LA5 showed strong binding to a single calcium ion with thermodynamic properties similar to previous reports (Fig. 3A, C).[5] However, LA4 reproducibly yielded a hyperbolic curve corresponding to a significantly weaker calcium affinity, K_D 163μM (Fig. 3B, Table 1), weaker than any module tested to date.[5,15,44,45] This result was consistent with the observation that HSQC spectra of LA4 showed the best dispersion and line widths at calcium concentrations of 5mM and above. Titrations with LA4 were repeated at pH 5.2 and calcium affinity was even weaker, with a K_D of 546μM (Fig. 3D).

To test whether calcium binding of LA4 would be different when it was connected to LA5, as it is in the full-length LDLR, we also tested calcium binding to LA45. The calcium-binding isotherm of LA45 showed strong binding to only a single calcium ion (Fig. 3E). Thermodynamic parameters from fitting to a two site model were consistent with one calcium ion binding to LA5 with high affinity, and the second binding with weak affinity to LA4. Due to the weak binding isotherm the thermodynamic parameters for the second calcium binding event could not be determined with a high degree of certainty.

Structure of LDLR LA45

The structure of LA45, refolded and purified under native HPLC conditions, was determined by NMR at pH 7.4. HSQC spectra of LA45 compared to those of each isolated module showed only weak perturbations resulting from linkage (Fig 5A, S1 supporting information).

While some of these chemical shift differences were not proximal to the linker, the result suggested that each module was structured independently. No changes in peak width or position were observed over a range of concentrations from 0.1 to 1.0mM indicating no significant self-association occurred under these experimental conditions. 3D ^{15}N-separated NOESY-HSQC, 3D ^{13}C-separated NOESY-HSQC and 3D ^{13}C-^{15}N separated HMQC-NOESY-HSQC ((H)CNH NOESY) spectra were analyzed with Ambiguous Restraint for Iterative Assignment (ARIA2) yielding a total of 2453 NOE based distance restraints (1850 unambiguous and 603 ambiguous). Amide cross peaks for residues 171–174 were not observed, and only weak NOEs were observed for this region in the 3D ^{13}C-separated NOESY-HSQC. Residual dipolar couplings (RDCs) (55) were obtained from the difference in dipolar coupling between aligned and unaligned samples from HSQC-IPAP experiments. Additional restraints for structural calculations included 50 chemical shift derived dihedral restraints (TALOS), 12 calcium binding restraints, 6 H-bonds, and 6 disulfide bonds (see Methods, Table 2).

The superposition of the 20 lowest energy structures on either LA4 or LA5 (Fig. 4) showed the structure of each module was well resolved, with backbone RMSDs of 0.38Å (LA4) and 0.28Å (LA5) (Table 2). No NOEs were observed between the two domains, however NOEs were observed between the linker residues R164 - Y167 and LA4. Although this constrained the N-terminal half of the 12 residue linker, the C-terminal part of the linker remained ill defined resulting in diverse inter-domain orientations within the ensemble. RDCs fit to each LA45 structure within the ensemble using PALES [46] gave a correlation between experimental and theoretical values >0.9, indicating that although highly variable, each relative domain orientation was consistent with the RDC data.

Backbone dynamics

NMR dynamics measurements were used to investigate whether intrinsic dynamics of these modules changes in the context of the linked module pair. H/D exchange experiments on LA45 conducted at pH 7.4 identified several amides in LA5 (E180, F181, C183, S185, I189, W193, R194, C195, D196, D200, C201, S205, D206, and E207) that were protected for hours, whereas all amides in LA4 were exchanged within minutes. R_1, R_2 relaxation rates and ^{15}N–{^{1}H} nuclear Overhauser effects (NOEs) were measured for LA4, LA5 and LA45 under identical conditions (Fig. S2, supporting information). R_2 relaxation rates for LA4 were higher than for LA5 (average 7.5 and 6.0 s^{-1} respectively), suggesting the presence of chemical exchange within LA4. Order parameters (S^2) from model-free fitting also show LA4 as being overall less ordered than LA5 (Fig. 5B). Estimates of rotational correlation time from R2/R1 indicate that the module pair undergo a degree of correlated tumbling (4.4+/− 0.8, 3.7 +/− 0.6, and 7.6 +/− 0.9 nsec for LA4, LA5 and LA45, respectively). Comparison of the order parameters of the isolated modules to the tandem LA45 revealed that regions at the calcium binding site in both LA4 (residues 145–151) and LA5 (residues 196–202) are more ordered in the module pair (Fig. 5B). Although most linker amides showed significant exchange broadening making it impossible to obtain relaxation data for this region, the ^{15}N–{^{1}H}NOE values for residues 166–170 in the N-terminal half of the linker were much higher than in LA4 alone indicating a significant degree of ordering of the first part of the linker in the domain pair (Fig. S2, supporting information). The ^{15}N–{^{1}H}NOE values decrease from the N-terminal to the C-terminal residues of the linker and the C-terminal half appears to retain a high degree of flexibility.

Specific dynamic changes arising from inter-domain connection were similar to the observed chemical shift perturbations arising from linkage. In the case of LA5 several amides showing large chemical shift perturbations upon linkage (H182, E187, G198, D200) also show significant differences in S^2 parameters and ^{15}N–{^{1}H}NOE values (Fig. 5B, Fig. S2, supporting information).

RAPD3 and ApoE(130-149) binding

Ligand titrations were used to characterize RAPD3 binding to each single module and to LA45 using Ubiquitin (Ub)-fused RAPD3 and Ub alone as the negative control (see Methods). HSQC spectra showed specific chemical shift perturbations within LA4 and LA5 upon binding of Ub-RAPD3 (Fig. S3, supporting information). The strongest shifts in LA45 (L143, D149, E158, H190, S192, G198, and the side chain ε1 of W144 and W193) were consistent with those seen in titrations with the individual modules. The affinities of LA4 and LA5 for Ub-RAPD3 calculated from these titrations yielded K_Ds of 49μM and 670μM respectively (Table 1). LA45 was fully bound even at 1:1 ratio to Ub-RAPD3, indicative of significantly tighter binding, as expected for the interaction of the two module pair.[47] Furthermore, LA45 remained bound to Ub-RAPD3 through size exclusion chromatography in a calcium dependent manner, as seen previously with the LA34•RAPD3 complex.[6]

NMR titrations of Ub-ApoE(130-149) with each isolated module and the module pair were also performed. Perturbations for Ub-ApoE(130-149) binding to the isolated LA4 and LA5 were essentially the same as those observed upon Ub-RAPD3 binding (Fig. S4, supporting information). The perturbations were also the same when titrating the linked module pair (Fig. 5C), however the binding affinity of both LA4 and LA5 was dramatically enhanced in the double module construct (405μM vs. 1090μM for LA4 and 730μM vs. 3880μM for LA5) (Fig. 6, Table 1). Notably, the two modules in the LA45 pair have a very distinct K_D, well outside of the error, suggesting that each module binds a separate molecule of Ub-ApoE(130-149).

Discussion

Structural similarity of LA modules

The structures of each individual module in LA45 are similar to the previously determined structures. The all atom r.m.s.d. of LA4 solved here compared to LA4 in LA34•RAPD3 was 1.74 Å,[6] and LA5 compared with the crystal structure of LA5 was 1.85Å. [4] Larger structural differences were seen when comparisons are made to the endosomal LDLR structure (Fig. 7).[2] The structural differences in the loop containing H190 (LA5) are likely attributed to the interaction of these regions with the β-propeller domain. [2] This same region undergoes one of the largest chemical shift perturbations upon ApoE(130-149) binding, strengthening the notion that they are involved in the ApoE-LDLR interaction. [21,48]

The linker between LA4 and LA5

Across species, evolution has conserved the length (12–14 residues) of the linker between LA4 and LA5 without conservation of any specific residues, which is typically seen for flexible linkers (Fig. S5, supporting information). Truncation of this linker significantly alters the interaction with LDL particles hinting that it may be required for the two modules to access distant epitopes on ligands such as multiple copies of ApoE on a lipoprotein surface.[17] The ApoE-binding pair of modules, 5 and 6, from the very low density lipoprotein receptor (VLDLR), also have a longer linker (9 residues) [52] but the sequence of this linker is conserved. It will be interesting to see whether LA56 in VLDLR shows similar dynamic properties.

Inter-domain crosstalk

It is not uncommon that weak inter-domain interactions govern relative orientations even in the absence of any observable inter-domain NOEs.[53,54] LA12 showed a preferred perpendicular orientation despite the absence of NOEs between the two domains and the larger τ_c of LA5 in LA56 (2.8 vs. 4.6nsec) was attributed to spatial occlusion.[14,55] The τ_c of LA5 in LA45 was also considerably longer (7.6 vs. 3.7nsec) possibly due to similar spatial

occlusion, which is remarkable because the linker between LA45 is three times longer than between LA5 and LA6. HYDRONMR calculations predict a τ_c of 9.2 +/− 0.9 nsec for the LA45 ensemble, still larger than the observed 7.6 nsec, again consistent with some but not complete restriction of the interdomain orientation. In an attempt to resolve the LA4-LA5 relative domain orientation ambiguity, we collected RDCs on the LA4-LA5 domain pair. Although the possible orientations are somewhat confined, due mostly to the restrains to the N-terminal half of the linker, the RDC restraints were consistent with a range of domain orientations. Together with the absence of inter-domain NOEs this result suggests that LA45 does not form rigid interdomain contacts, with only transient interactions limiting its domain motions.

Functional consequences for ligand binding

Both NMR and cryo-EM studies have shown that many LA modules act as isolated units, and it has been suggested that this provides flexibility to bind a diversity of ligands.[12,13,14,15,55] Despite the long, relatively flexible linker connecting them, the LA45 modules appear to be influenced by the presence of their neighbors. Weak inter-molecular effects had been previously observed for module pairs, [55] but consequences of this type of cross-talk have not yet been examined. Here we present evidence that ligand affinity correlates with the effects of the observed inter-module crosstalk.

Our previous functional studies showed that LA4 primarily interacts with the canonical ApoE receptor binding region (ApoE 130-149).[21] The backbone dynamics of LA4 presented here show changes at residues 142–152, residues critical for ApoE binding, when linked to LA5 (Fig. 5B). It is likely that these effects are at least partly responsible for the observed enhancement of ApoE(130-149) binding by the module pair as compared to isolated LA4. The same titrations showed that linkage also leads to changes at the LA5 ligand binding site as well, although the ApoE(130-149) may not represent the relevant binding partner as LA5 is thought to bind a distinct epitope involving ApoE residues 186–193.[21] Interestingly the modules in both LA12 and LA56 undergo minor chemical shift perturbations when linked, [13,15] and weak inter-domain crosstalk may be occurring in these module pairs as well.

Functional consequences of the weak calcium affinity of LA4

LA4 exhibited the lowest affinity for calcium compared to all other members of this class of protein modules.[45]. Calcium binding to LA4 has only previously been tested using a four repeat construct LA3456,[18] in which the weak binding isotherm of this particular module is likely to be miniscule, just as we observed in LA45. Since LA modules depend on calcium coordination for their native fold,[11] the weak calcium affinity may be the reason this repeat refolds poorly,[13] and may be related to the higher backbone dynamics in LA4 compared to LA5 and other repeats. However, LA1 and LA2, which have similar affinities for calcium, have very different backbone dynamics.[8,13,14] Another possibility is that the octahedral geometry for the calcium binding site in LA4 is distorted, possibly by P150. A Pro at this position is rare among LA modules in the LDLR family. In the case of LA5, G198 may offset the distortion imposed by P199 (at the equivalent position of P150) to allow for more favorable calcium binding geometry.

The weak calcium affinity of LA4 may have functional relevance regarding ligand release. Calcium ion occupancy is necessary for LDL modules to bind ligands.[11] LA4 would be over 90% calcium bound at serum calcium ion levels of around 2mM,[49] however at endosomal calcium ion concentration of 10μM,[50] it would be only 5% bound. The acidic environment in the endosome further reduces the affinity, resulting in a calcium ion occupancy for LA4 near zero, which would cause, or at least contribute to ligand release. These results are

consistent with the recent model that both low pH and low Ca^{+2} concentration trigger LDL release,[3] but indicate that LA4 rather than LA5, as suggested previously,[51] is the critical module that triggers ligand release in the endosome.

Supplementary Material

Refer to Web version on PubMed Central for supplementary material.

Acknowledgments

This work was supported by NIH grant RO1 AG025343. MG was supported by the Heme and Blood Proteins Training Grant, T32-DK007233.

We wish to thank Joseph Noel at the Salk Institute for the pHis8 vector and Tracy M. Handel and Peter Domaille for help with the NMR experiments.

Abbreviations

GST	Glutathione S-transferase
RAP	Receptor Associated Protein
CR	complement repeat
LA	Ligand binding repeat
NMR	nuclear magnetic resonance
MALDI-TOF	matrix assisted laser desorption ionization time of flight
LDLR	low density lipoprotein receptor
HPLC	high performance liquid chromatography
HSQC	heteronuclear single quantum coherence
ITC	isothermal titration calorimetry
NOE	nuclear Overhauser effect
τ_c	rotational correlation time

References

1. Blacklow SC. Versatility in ligand recognition by LDL receptor family proteins: advances and frontiers. Curr Opin Struct Biol. 2007; 17:419–426. [PubMed: 17870468]
2. Rudenko G, Henry L, Henderson K, Ichtchenko K, Brown MS, Goldstein JL, Deisenhofer J. Structure of the LDL receptor extracellular domain at endosomal pH. Science. 2002; 298:2353–2358. [PubMed: 12459547]
3. Zhao Z, Michaely P. The Role of Calcium in Lipoprotein Release by the Low-Density Lipoprotein Receptor. Biochemistry. 2009; 48:7313–7324. [PubMed: 19583244]
4. Fass D, Blacklow S, Kim PS, Berger JM. Molecular basis of familial hypercholesterolaemia from structure of LDL receptor module. Nature. 1997; 388:691–693. [PubMed: 9262405]
5. Simonovic M, Dolmer K, Huang W, Strickland DK, Volz K, Gettins PGW. Calcuim Coordination and pH dependence of the calcium affinity of ligand-binding repeat CR7 from the LRP. Comparision with related domains from the LRP and the LDL receptor. Biochemistry. 2001; 40:15127–15134. [PubMed: 11735395]
6. Fisher C, Beglova N, Blacklow SC. Structure of an LDLR-RAP complex reveals a general mode for ligand recognition by lipoprotein receptors. Mol Cell. 2006; 22:277–283. [PubMed: 16630895]

7. Daly NL, Scanlon MJ, Djordijevic JT, Kroon PA, Smith R. Three-dimernsional structure of a cysteine-rich repeat from the low-density lipoprotein receptor. Proc Natl Acad Sci USA. 1995; 92:6334–6338. [PubMed: 7603991]
8. Daly NL, Djordjevic JT, Kroon PA, Smith R. Three-dimensional structure of the second cysteine-rich repeat from the human low-density lipoprotein receptor. Biochemistry. 1995; 34:14474–14481. [PubMed: 7578052]
9. North CL, Blacklow SC. Solution structure of the sixth LDL-A module of the LDL receptor. Biochem J. 2000; 39:2564–2571.
10. Guo Y, Yu X, Rihani K, Wang QY, Rong L. The role of a conserved acidic residue in calcium-dependent protein folding for a low density lipoprotein (LDL)-A module: implications in structure and function for the LDL receptor superfamily. J Biol Chem. 2004; 279:16629–16637. [PubMed: 14749324]
11. Blacklow SC, Kim PS. Protein folding and calcium binding defects arising from familial hypercholesterolemia mutations of the LDL receptor. Nat Struc Biol. 1996; 3:758–762.
12. Jeon H, Shipley GG. Vesicle-reconstituted low density lipoprotein receptor. Visualization by cryoelectron microscopy. J Biol Chem. 2000; 275:30458–30464. [PubMed: 10889196]
13. Bieri S, Atkins AR, Lee HT, Winzor DJ, Smith R, Kroon PA. Folding, Calcium Binding, and Structural Characterization of a Concatemer of the First and Second Ligand-Binding Modules of the Low-Density Lipoprotein Receptor. Biochemistry. 1998; 37:10994–11002. [PubMed: 9692993]
14. Kurniawan ND, Atkins AR, Bieri S, Brown CJ, Brereton IM, Kroon PA, Smith R. NMR structure of a concatemer of the first and second ligand-binding modules of the human low-density lipoprotein receptor. Protein Sci. 2000; 9:1282–1293. [PubMed: 10933493]
15. North CL, Blacklow SC. Structural independence of ligand-binding modules five and six of the LDL receptor. Biochem J. 1999; 38:3926–3935.
16. Esser V, Limbird LE, Brown MS, Goldstein JL, Russell DW. Mutational analysis of the ligand binding domain of the low density lipoprotein receptor. J Biol Chem. 1988; 263:13282–13290. [PubMed: 3417658]
17. Russell DW, Brown MS, Goldstein JL. Different combinations of cysteine-rich repeats mediate binding of low density lipoprotein receptor to two different proteins. J Biol Chem. 1989; 264:21682–21688. [PubMed: 2600087]
18. Fisher C, Abdul-Aziz D, Blacklow SC. A two-module region of the low-density lipoprotein receptor sufficient for formation of complexes with apolipoprotein E ligands. Biochem J. 2004; 43:1037–1044.
19. Yamamoto T, Ryan RO. Domain swapping reveals that low density lipoprotein (LDL) type A repeat order affects ligand binding to the LDL receptor. J Biol Chem. 2009; 284:13396–133400. [PubMed: 19329437]
20. Ren G, Rudenko G, Ludtke SJ, Deisenhofer J, Chiu W, Pownall HJ. Model of human low-density lipoprotein and bound receptor based on cryoEM. Proc Natl Acad Sci U S A. 2010; 107:1059–1064. [PubMed: 20080547]
21. Guttman M, Prieto JH, Croy JE, Komives EA. Decoding of lipoprotein - receptor interactions; Properties of ligand binding modules governing interactions with ApoE. Biochemistry. 2010; 49:1207–1216. [PubMed: 20030366]
22. Jez MJ, Ferrer J, Bowman ME, Dixon RA, Noel JP. Dissection of Malonyl-Coenzyme A Decarboxylation from Polyketide Formation in the Reaction Mechanism of a Plant Polyketide Synthase. Biochemistry. 2000; 39:890–902. [PubMed: 10653632]
23. Grzesiek S, Bax A. An Efficient Experiment For Sequential Backbone Assignment of Medium-Sized Isotopically Enriched Proteins. J Magn Reson. 1992; 99:201–207.
24. Grzesiek S, Bax A. Correlating backbone amide and side chain resonances in larger proteins by multiple relayed triple resonance NMR. J Am Chem Soc. 1992; 114:6291–6293.
25. Kay LE, Ikura M, Tschudin R, Bax A. Three-dimensional triple-resonance NMR spectroscopy of isotopically enriched proteins. J Magn Reson. 1990; 89:496–514.

26. Clowes RT, Boucher W, Hardman CH, Domaille PJ, Laue ED. A 4D HCC(CO)NNH experiment for the correlation of aliphatic side-chain and backbone resonances in 13C/15N-labelled proteins. J Biomol NMR. 1993; 3:349–354.
27. Talluri S, Wagner G. An Optimized 3D NOESY–HSQC. J Magn Reson. 1996; 112:200–205.
28. Bax A, Clore GM, Gronenborn AM. Proton-proton correlation via isotropic mixing of carbon-13 magnetization, a new three-dimensional approach for assigning proton and carbon-13 spectra of carbon-13-enriched proteins. J Magn Reson. 1990; 88:425–431.
29. Ikura M, Kay LE, Bax A. Improved three-dimensional 1H-13C-1H spectroscopy of a 13C-labeled protein using constant-time evolution. J Biomol NMR. 1991; 1:299–304. [PubMed: 1841700]
30. Zuiderweg ERP, McIntosh LP, Dahlquist FW, Fesik SW. Three-dimensional carbon-13-resolved proton NOE spectroscopy of uniformly carbon-13-labeled proteins for the NMR assignment and structure determination of larger molecules. J Magn Reson. 1990; 86:210–216.
31. Delaglio F, Grzesiek S, Vuister G, Zhu G, Pfeifer J, Bax A. NMRPipe: a multidimensional spectral processing system based on UNIX pipes. J Biomol NMR. 1995; 6:277–293. [PubMed: 8520220]
32. Goddard, TD.; Kneller, DG. SPARKY 3. University of California; San Francisco:
33. Cordier F, Dingley AJ, Grzesiek S. A doublet-separated sensitivity-enhanced HSQC for the determination of scalar and dipolar one-bond J-couplings. J Biomol NMR. 1999; 13:175–180. [PubMed: 10070758]
34. Rieping W, Habeck M, Bardiaux B, Bernard A, Malliavin TE, Nilges M. ARIA2: automated NOE assignment and data integration in NMR structure calculation. Bioinformatics. 2007; 23:381–382. [PubMed: 17121777]
35. Cornilescu G, Delaglio F, Bax A. Protein backbone angle restraints from searching a database for chemical shift and sequence homology. J Biomol NMR. 1999; 13:298–302.
36. Warren JJ, Moore PB. A Maximum Likelihood Method for Determining DaPQ and R for Sets of Dipolar Coupling Data. J Magn Res. 2001; 149:271–275.
37. Brunger AT. Version 1.2 of the Crystallography and NMR System. Nature Protocols. 2007; 2:2728–2733.
38. Jensen GA, Andersen OM, Bonvin AM, Bjerrum-Bohr I, Etzerodt M, Thøgersen HC, O'Shea C, Poulsen FM, Kragelund BB. Binding site structure of one LRP-RAP complex: implications for a common ligand-receptor binding motif. J Mol Biol. 2006; 362:700–716. [PubMed: 16938309]
39. Maiti R, Van Domselaar GH, Zhang H, Wishart DS. SuperPose: a simple server for sophisticated structural superposition. Nucleic Acids Res. 2004; 32:590–594. [PubMed: 14752047]
40. DeLano, WL. The PyMOL Molecular Graphics System. DeLano Scientific; San Carlos, CA, USA: 2002.
41. Cordier F, Caffrey M, Brutscher B, Cusanovich MA, Marion D, Blackledge M. Solution structure, rotational diffusion anisotropy and local backbone dynamics of Rhodobacter capsulatus cytochrome c2. J Mol Biol. 1998; 281:341–361. [PubMed: 9698552]
42. García de la Torre J, Huertas ML, Carrasco B. HYDRONMR: prediction of NMR relaxation of globular proteins from atomic-level structures and hydrodynamic calculations. J Magn Reson. 2000; 147:138–146. [PubMed: 11042057]
43. Hoffman RMB, Li MX, Sykes BD. The Binding of W7, an Inhibitor of Striated Muscle Contraction, to Cardiac Troponin C. Biochemistry. 2005; 44:15750–15759. [PubMed: 16313178]
44. Andersen OM, Vorum H, Honoré B, Thøgersen HC. Ca2+ binding to complement-type repeat domains 5 and 6 from the low-density lipoprotein receptor-related protein. BMC Biochemistry. 2003; 4:7, 1–7. [PubMed: 12921543]
45. Rudenko G, Deisenhofer J. The low-density lipoprotein receptor: ligands, debates and lore. Curr Opin Struct Biol. 2003; 13:683–689. [PubMed: 14675545]
46. Zweckstetter M. NMR: prediction of molecular alignment from structure using the PALES software. Nat Protoc. 2008; 3:679–690. [PubMed: 18388951]
47. Andersen OM, Schwarz FP, Eisenstein E, Jacobsen C, Moestrup SK, Etzerodt M, Thøgersen HC. Dominant thermodynamic role of the third independent receptor binding site in the receptor-associated protein RAP. Biochem J. 2001; 40:15408–15417.

48. Abdul-Aziz D, Fisher C, Beglova N, Blacklow SC. Folding and binding integrity of variants of a prototype ligand-binding module from the LDL receptor possessing multiple alanine substitutions. Biochem J. 2005; 44:5075–5085.

49. Marshall, WJ. Clinical Chemistry. Mosby; London: 1995. (ed., r., Ed.)

50. Gerasimenko JV, Tepikin AV, Petersen OH, Gerasimenko OV. Calcium uptake via endocytosis with rapid release from acidifying endosomes. Curr Biol. 1998; 8:1335–1338. [PubMed: 9843688]

51. Arias-Moreno X, Velazquez-Campoy A, Rodríguez JC, Pocovi M, Sancho J. Mechanism of low density lipoprotein (LDL) release in the endosome: implications of the stability and Ca2+ affinity of the fifth binding module of the LDL receptor. J Biol Chem. 2008; 283:22670–22679. [PubMed: 18574243]

52. Ruiz J, Kouiavskaia D, Migliorini M, Robinson S, Saenko EL, Gorlatova N, Li D, Lawrence D, Hyman BT, Weisgraber KH, Strickland DK. The apoE isoform binding properties of the VLDL receptor reveal marked differences from LRP and the LDL receptor. J Lipid Res. 2005; 46:1721–1731. [PubMed: 15863833]

53. Murphy JM, Hansen FD, Wiesner S, Muhandiram RD, Borg M, Smith MJ, Sicheri F, Kay LE, Forman-Kay JD, Pawson T. Structural Studies of FF Domains of the Transcription Factor CA150 Provide Insights into the Organization of FF Domain Tandem Arrays. J Mol Biol. 2009; 393:409–424. [PubMed: 19715701]

54. Spitzafden C, Grant RP, Mardon HJ, Campbell ID. Module-Module Interactions in the Cell Binding Region of Fibronectin: Stability, Flexibility and Specificity. J Mol Biol. 1997; 265:565–579. [PubMed: 9048949]

55. Beglova N, North CL, Blacklow SC. Backbone dynamics of a module pair from the ligand-binding domain of the LDL receptor. Biochemistry. 2001; 6:2808–2815. [PubMed: 11258891]

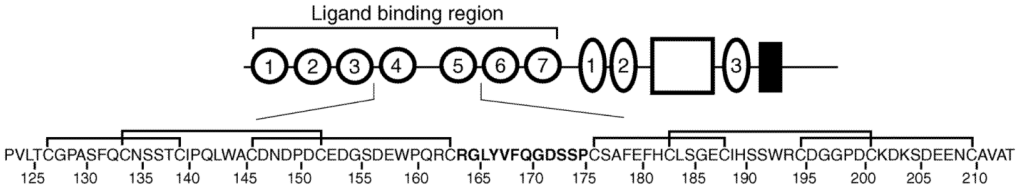

Figure 1.

Schematic diagram of the LDL receptor with ligand binding modules (circles), EGF like repeats (ovals), β-propeller domain (open rectangle), and transmembrane domain (filled rectangle). The sequence of LA45 with linker (bold) is also shown with residues numbered according to the mature protein sequence with bold lines indicating disulfide bonds.

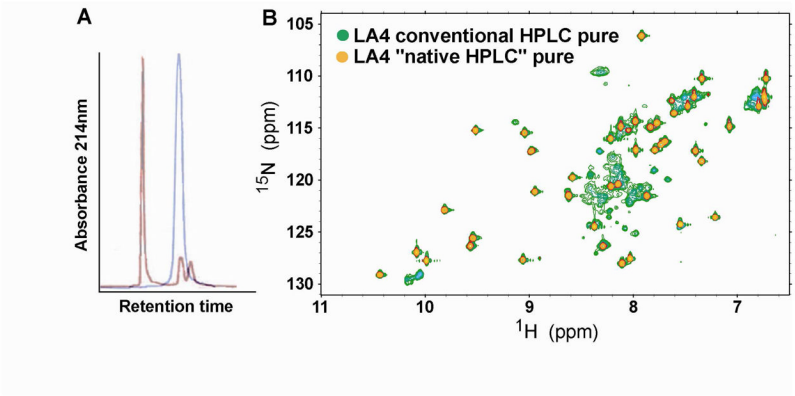

Figure 2.

(A) Overlay of the analytical HPLC traces of purified LA4 in either 0.1% TFA (blue) or 10mM NH_4OAc (pH 5.5) with 5mM $CaCl_2$ (red). (B) Overlay of the HSQC spectra of LA4 after conventional HPLC purification (green) or after HPLC purification under native (calcium bound) conditions (gold).

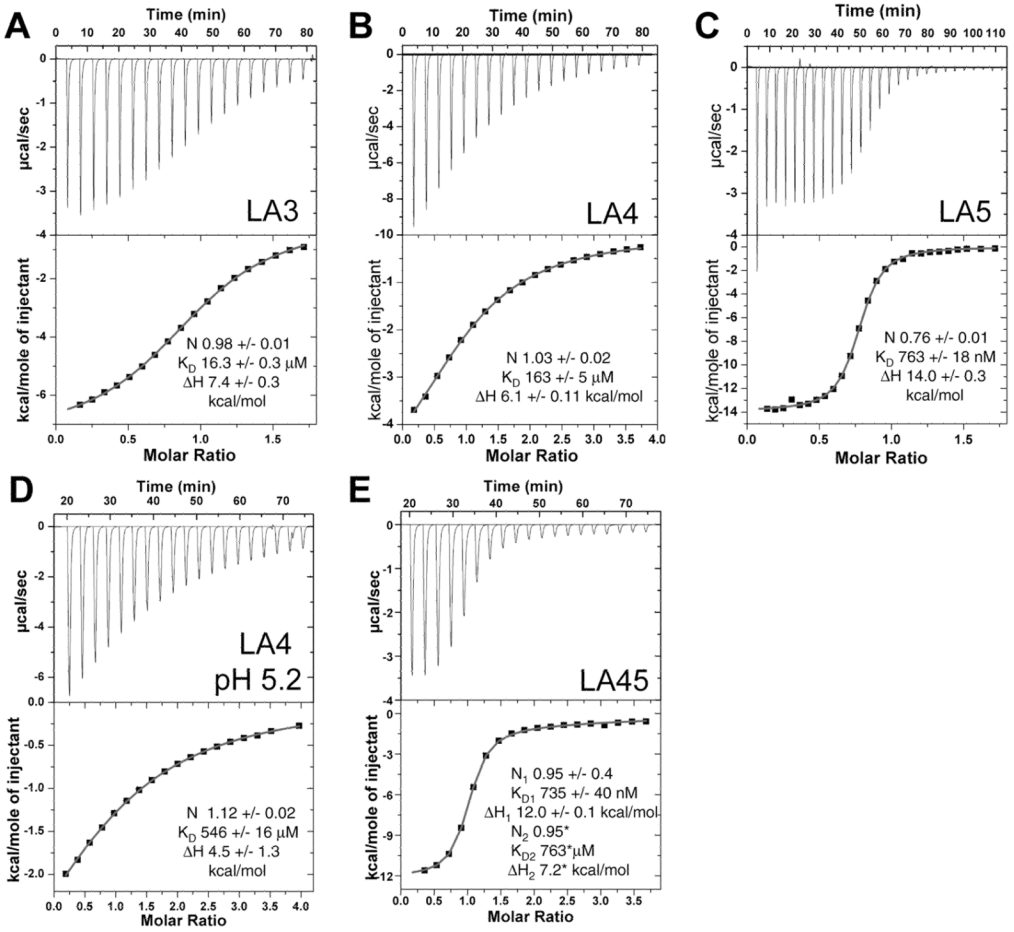

Figure 3.
Calcium binding isotherms for (A) LA3, (B) LA4, (C) LA5, (D) LA4 at pH 5.2 and (E) LA45 at pH 7.4.

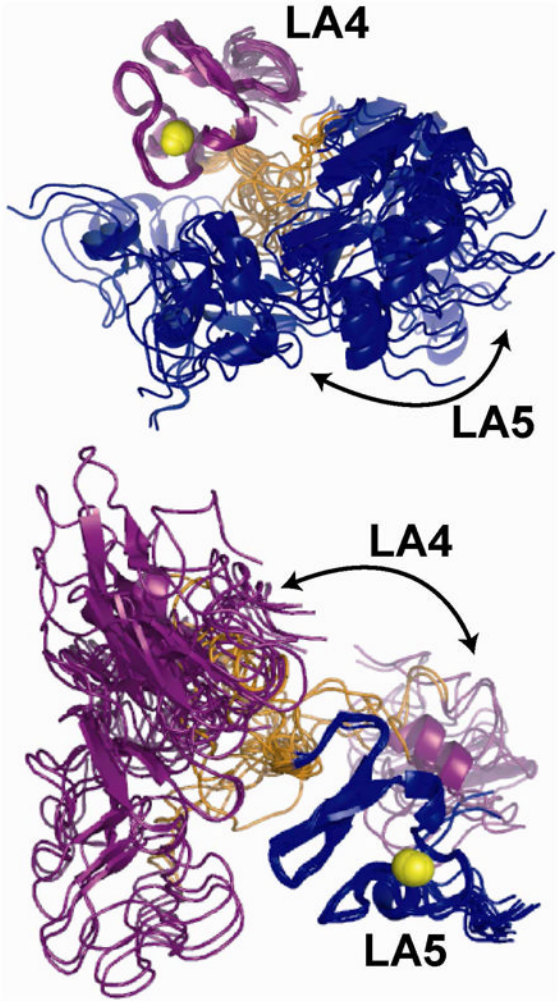

Figure 4.
Superposition of the 20 lowest energy structures of LA45 with LA4 (purple), linker (orange), LA5 (blue), and calcium ions (yellow spheres). Structures are aligned either to residues 127–163 of LA4 (top), or residues 176–210 of LA5 (bottom).

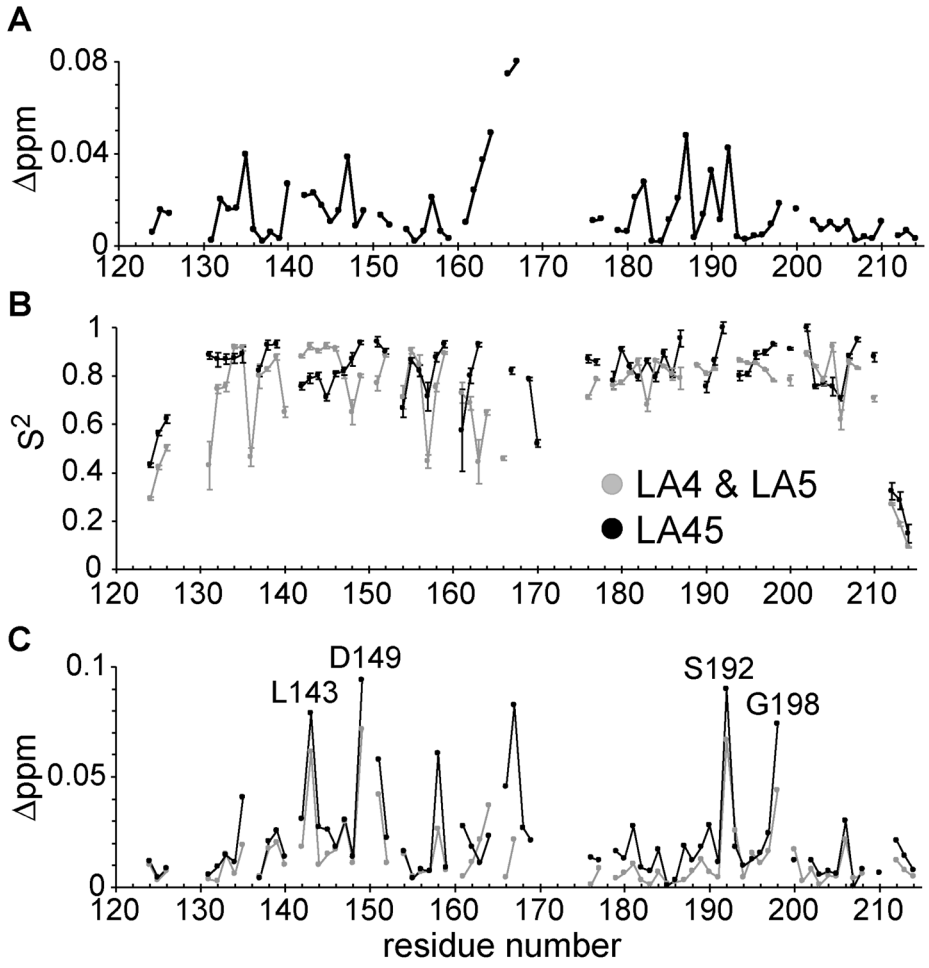

Figure 5.

A) Chemical shift differences (^{1}H and ^{15}N, see methods) between LA45 and each isolated module. B) Order parameters (S^2) obtained from model free fitting of relaxation data for LA45 (black) and isolated LA4 and LA5 (grey) (R1, R2 and ^{15}N–{^{1}H}NOE are shown in Supp. Fig 2. C). Chemical shift perturbations of LA45 (black) and both isolated modules (grey) upon binding ApoE(130-149). Residues showing the largest changes are labeled. ^{15}N–{^{1}H}NOE values for LA45 and isolated modules with the same coloring as (B). Data for regions 142–149 (LA4) and 179–200 (LA5) are enlarged and shown as insets.

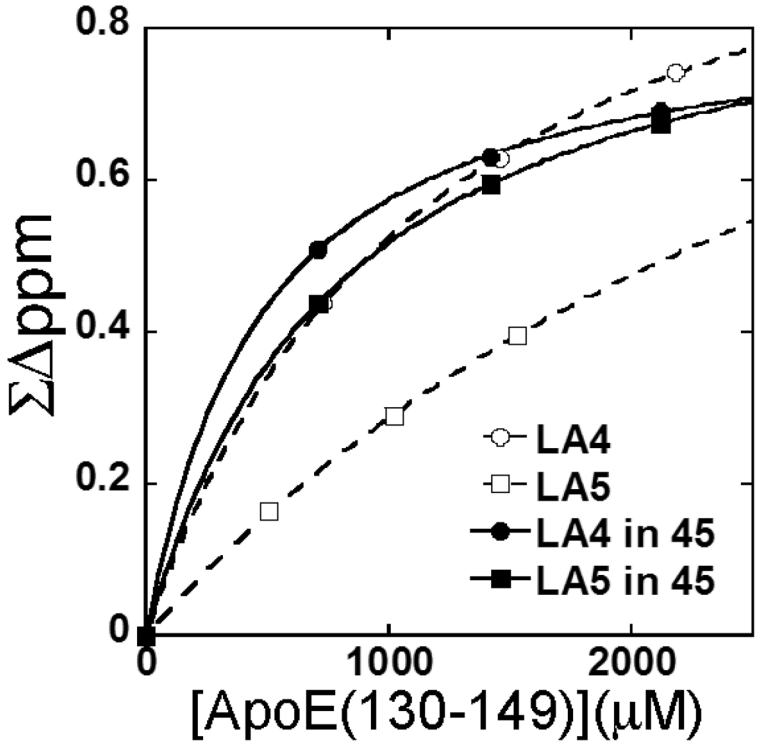

Figure 6.
Titration fits of Ub-ApoE(130-149) binding isolated LA4 (○) isolated LA5 (□), LA4 in LA45 (●) and LA5 in LA45 (■). Plots are sum total of the magnitude of the perturbations (in ppm) plotted against the concentration of ApoE(130-149).

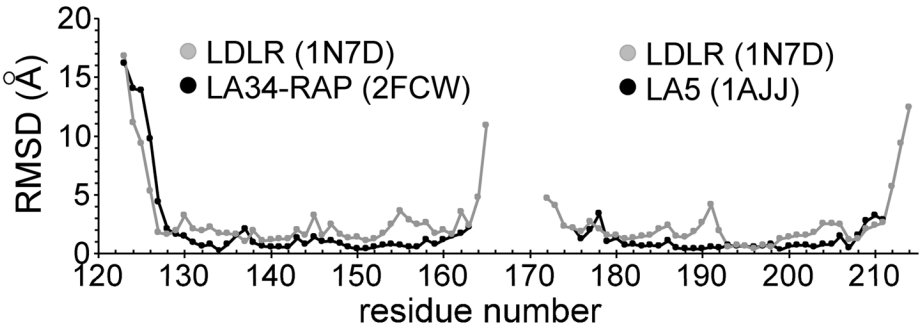

Figure 7.

Root mean square deviations (backbone only) of the structure of LA45 determined here by NMR at physiological pH as compared to the structure of LA45 from the crystal structure of the LDLR at endosomal pH (black) LA4 from pdb accession code 2fcw and LA5 from pdb accession code 1ajj (grey).

Table 1

Binding affinities of calcium and ligands to LDLR fragment pairs

Ligand	LA	K_D (μM)
Calcium[1]	LA3 alone	16 ± 0.25
	LA4 alone	173 ± 14
	LA5 alone	0.76 ± 0.05
	LA4 (in LA45)	763 ± ND
	LA5 (in LA45)	0.74 ± 0.04
	LA4 (pH 5.2)	546 ± 16
RAPD3[2]	LA4 alone	49 ± 3
	LA5 alone	670 ± 26
Apoe(130-149)[2]	LA4 alone	1090 ± 90
	LA4 in LA45	405 ± 41
	LA5 alone	3880 ± 290
	LA5 in LA45	730 ± 160

[1] From Isothermal titration calorimetry experiments

[2] From NMR titration experiments

ND Uncertainty very high due to weak binding isotherm

Table 2

NMR structural statistics

NMR Constraints	
Distance Constraints	2453
Intra-residue	389
Sequential ($\|i - j\| = 1$)	499
Medium-range ($\|i - j\| < 4$)	424
Long-range ($\|i - j\| > 5$)	538
Ambiguous	603
Hydrogen bonds	6
Dihedral angle restraints	50
Residual dipolar coupling restraints	55
Structural Statistics (20 Structures)	
rmsd from idealized covalent geometry	
Bond lengths (Å)	0.0016 +/− 0.00013
Bond angles (°)	0.3290 +/− 0.02219
Impropers (°)	0.2044 +/− 0.02155
rmsd from distance constraints (Å)	0.0414 +/− 0.00359
rmsd from dihedral Angle Constraints (°)	0.6222 +/− 0.70447
Coordinate Precision	
Average pairwise rmsd (residues 127–163) (Å) (LA4)	
All backbone atoms	0.38 +/− 0.11
All heavy atoms	0.58 +/− 0.13
Average pairwise rmsd (residues 176–210) (Å) (LA5)	
All backbone atoms	0.28 +/− 0.13
All heavy atoms	0.51 +/− 0.15
Ramachandran Plot Statistics (residues 127–163, 176–210) (%)	
Most favored regions	64.4
Additionally allowed regions	30.7
Generously allowed regions	4.6
Disallowed regions	0.2